
Deep Reinforcement Learning for Time-Critical Wilderness Search And Rescue Using Drones

Jan-Hendrik Ewers

Aerospace Sciences Research Division
School of Engineering
University of Glasgow
j.ewers.1@research.gla.ac.uk

David Anderson

Aerospace Sciences Research Division
School of Engineering
University of Glasgow
dave.anderson@glasgow.ac.uk

Douglas Thomson

Aerospace Sciences Research Division
School of Engineering
University of Glasgow
douglas.thomson@glasgow.ac.uk

Abstract

Traditional search and rescue methods in wilderness areas can be time-consuming and have limited coverage. Drones offer a faster and more flexible solution, but optimizing their search paths is crucial. This paper explores the use of deep reinforcement learning to create efficient search missions for drones in wilderness environments. Our approach leverages a priori data about the search area and the missing person in the form of a probability distribution map. This allows the deep reinforcement learning agent to learn optimal flight paths that maximize the probability of finding the missing person quickly. Experimental results show that our method achieves a significant improvement in search times compared to traditional coverage planning and search planning algorithms. In one comparison, deep reinforcement learning is found to outperform other algorithms by over 160%, a difference that can mean life or death in real-world search operations. Additionally, unlike previous work, our approach incorporates a continuous action space enabled by cubature, allowing for more nuanced flight patterns.

1 Introduction

Wilderness Search and Rescue (WiSAR) operations in Scotland's vast and often treacherous wilderness pose significant challenges for emergency responders. To combat this, Police Scotland Air Support Unit (PSASU) and Scottish Mountain Rescue (SMR) regularly use helicopters to assist in search operations^[2]. However, the deployment of helicopters can be slow, especially in the Scottish Isles where the PSASU's Eurocopter EC135 based in Glasgow can take multiple hours to arrive. Additionally, operating helicopters is extremely costly.

Drones, also known as unmanned aerial vehicles, offer a cost-effective and agile solution for aerial search. Both PSASU and SMR are placing small fleets of drones around Scotland for rapid deployment in a WiSAR scenario. These fleets will never replace the requirement for a helicopter due to the inherent lifting disparities between the two platforms but will ensure that the search can begin as soon as possible. Successfully utilizing drones in WiSAR requires careful planning^[30].

The current approach to flying drones for PSASU is the pilot-observer model where two personnel are required at a minimum per drone. In this setup, the observer is in charge of maintaining visual

line of sight at all times whilst the pilot can fly the drone and inspect the live camera feed. Koester et al.^[18] identifies that a foot-based searcher has a higher detection rate when not in motion, similar to the behaviour exhibited by pilots who will fly to a location then stop and pan the camera^[6]. The cognitive load between in-motion and static search is evidently a barrier, as having the drone in motion at all times will lead to more area coverage which could lead to saved lives.

Another class of algorithm that has surpassed human abilities in highly complex tasks is Deep Reinforcement Learning (DRL), a subset of machine learning. DRL has been successfully applied to playing video games^[22,25] and has achieved championship-level drone racing^[16]. The ability of DRL to generalize the problem and make decisions based on extensive training allows it to provide unique solutions that other algorithms may not be able to achieve.

At the core of the problem, WiSAR mission planning involves the effective use of a priori data, such as the place last seen, age, and fitness levels of the missing person. This information can be used to generate a Probability Distribution Map (PDM)^[6,14,29], which describes the probability of detecting the missing person at a given location and informs the search stage of the mission.

Our research hypothesis is that by using DRL combined with a continuous PDM, a more effective search path can be created. The intent of using DRL is to allow better PDM exploration whilst the continuous PDM prevents undesired noisy rewards^[11,9] during training. We benchmark our algorithm against work from Lin and Goodrich^[20], and a standard lawnmower pattern^[32].

The contribution of this research to the field is the unique usage of a PDM as part of the observation space for the DRL agent. Similar DRL algorithms by Talha et al.^[33] and Peake et al.^[26] explore the environment whilst searching and do not have the complete PDM at the beginning. Another DRL search algorithm from Ebrahimi et al.^[5] localizes missing people using radio signal strength indexes which, again, does not have the a priori data present that our method does. Furthermore, this is the first search algorithm that uses a continuous PDM during the evaluation stage, enabling a continuous action space whilst maintaining accurate probability integration^[8].

Further related work is discussed in Section 2, and the methodology is presented in Section 3. Results are shown in Section 4 with limitations being discussed in Section 5, and a conclusion is drawn in Section 6.

2 Related Work

Coverage planning algorithms have been around for decades^[10] in various forms with the most well-known, and intuitive, being the parallel swaths (also known as lawnmower or zig-zag) pattern. This guarantees complete coverage of an entire area given enough time. However, for WiSAR applications, reducing the time to find is substantially more important than searching the entire area. In order to break away from the complete coverage problem definition, a different objective needs to be defined. This comes in the form of maximizing the accumulated probability over a PDM. PDMs can be created in a number of ways such as through geometrical approaches^[15], agent-based methods^[14], or using machine learning^[29]. All of these attempt to model the probability of where a lost person is located using information such as where they were last seen, age, sex, and more. This is a powerful tool in narrowing down a larger search area into something more manageable.

Lin and Goodrich^[20] approach the search planning problem by using a gradient descent algorithm in the form of Local Hill Climbing (LHC) that can advance into any of the surrounding eight cells. However, LHC alone is not sufficient because Waharte and Trigoni^[34] found that this class of algorithm does not perform well due to their propensity in getting stuck around local maxima. For this reason Lin and Goodrich^[20] introduces the notion of global warming to break out of local maxima. This raises the zero probability floor sequentially a number of times, storing the paths and then re-assessing them given the original PDM. Through this, and a convolution-based tie-breaking scheme, LHC_GW_CONV (local hill climb, global warming, convolution) is shown to have very favourable results. Yet, at every time step only the adjacent areas are considered. This means that areas of higher total probability may not ever be considered until the current one is entirely covered.

Another approach to overcome this problem is to use a dynamic programming-based approach. Snyder et al.^[31] uses Dijkstra's algorithm by identifying the points of highest probability on the PDM and applying the point-to-point path planning algorithm from the start, to these points, and then finally back to the start when the endurance limit is equal to the distance back. The reward function

along the route is the probability seen by advancing into that position. Like LHC.GW.CONV, this is an iterative algorithm allowing movement into one of the surrounding cells before repeating the process. Whilst this approach maximises the probability on the route towards the global maxima, this does not consider other areas which could yield more total probability.

In order to consider the area as a whole, sampling-based optimisation approaches have been applied to the problem. Morin et al.^[24] uses ant colony optimisation with a discrete PDM and Ewers et al.^[7] uses both genetic algorithm and particle swarm optimisation with a pseudo-continuous PDM. Both are capable of finding solutions that do not necessarily need to include the global maxima, however due to the nature of sampling-based optimisation problems they are prone to long computation times to converge on a solution.

A core problem with the previously mentioned algorithms is the inability to consider the PDM as a whole when making decisions. Being able to prioritise long-term goals over short-term gains is a key feature of DRL. This strand of machine learning couples classic reinforcement learning and neural networks to learn the optimal action based on an observation.

DRL is being used extensively for mission planning such as by Yuksek et al.^[37] who used proximal policy optimisation to create a trajectory for two drones to avoid no-fly-zones whilst tracking towards the mission objective. This approach has defined start and target locations, however the uses of no-fly-zones with constant radius is analogous to an inverted PDM. Peake et al.^[26] uses Recurrent-DDQN for target search in conjunction with A2C for region exploration with a single drone to find missing people. This method does not use any a priori information but rather explores the area in real time. However, in the end it does not outperform parallel swaths by a significant margin as would be expected by a more complex solution. This shows that DRL is a suitable approach to the search-over-PDM problem that a WiSAR mission requires.

A core aspect of DRL is having a fully observable environment such that the policy can infer why the action resulted in the reward. This is known as the markov decision process and is critical. Thus, being able to represent the PDM effectively is a primary goal. Whilst images can be used as inputs for DRL, as done by Mnih et al.^[22] to play Atari 2600 computer games, the typically large dimension can be prohibitive. Being able to represent the same information in a more concise manner reduces the observation space size resulting in lower training overhead. However, since PDM generation algorithms typically create discrete maps^[29,15,14], finding a different representation is required. To go from a discrete to continuous PDM, Lin and Goodrich^[21] uses a gaussian mixture model to represent the PDM as a sum of bivariate Gaussians. Yao et al.^[36] uses a similar approach to approximate a univariate Gaussian along a river for search planning. This can be easily used to numerically represent the numerous bivariate Gaussian parameters in an array which is a suitable format for a DRL observation.

An additional benefit of having a continuous representation is the performance increase, in both noise and speed, of calculating the accumulated probability as evaluated by Ewers et al.^[8]. It was found that the sampling-based approach typically used in conjunction with discrete PDMs only resulted in better speeds at low dimensions compared to the cubature method^[4]. It was also found that the cubature method always resulted in lower noise in the test cases where the sampling-based method was faster. This is beneficial to ML in general, as higher quality training data is always desired.

There are many DRL algorithms to choose from with proximal policy optimisation^[28] and Soft Actor-Critic (SAC)^[12] being some of the most prevalent in the literature^[37,23,35]. Mock and Muknahallipatna^[23] found that proximal policy optimisation performed well for low dimension observation spaces, whilst SAC performed much better for larger ones. The need for a large observation space comes from the fact that the policy would need have a sense of memory regarding where it had been to encounter *unseen* probability to satisfy the markov decision process that underpins DRL. Mock and Muknahallipatna^[23] found that a recurrent architecture was comparable to including previous states in the observation (also known as frame stacking). This shows that frame-stacking with SAC is a suitable DRL architecture for the current problem.

3 Method

All parameters used in this study can be found in Appendix A.

3.1 Modelling

3.1.1 Environment

The drone within the environment is modelled as a simple heading control model with a constant step size λ . It is assumed that any drone executing this mission can perfectly track the waypoints through its controller or operator. Thus, the position vector $\mathbf{x} \in \mathbb{R}^2$ is updated via

$$\mathbf{x}_{t+1} = \mathbf{x}_t + \lambda \begin{bmatrix} \cos u_t \\ \sin u_t \end{bmatrix} \quad (1)$$

$$u_t = \pi(a_t + 1) \quad (2)$$

where $a_t \in [-1, 1]$ is the policy action at time-step t .

3.1.2 PDM

The PDM is modelled as a sum of N_{gaussian} bivariate Gaussians^[36] such that a point on the ground at coordinate $\mathbf{x} \in \mathbb{R}^2$ has a probability of containing the missing person

$$p(\mathbf{x}) = \frac{1}{N_{\text{gaussian}}} \sum_{i=0}^{N_{\text{gaussian}}} \frac{\exp[-\frac{1}{2}(\mathbf{x} - \mu_i)^T \sigma_i^{-1}(\mathbf{x} - \mu_i)]}{\sqrt{4\pi^2 \det \sigma_i}} \quad (3)$$

$$\forall i \in [0, G], \mu_i \sim \mathcal{U}([x_{\min}, x_{\max}], [y_{\min}, y_{\max}]) \quad (4)$$

where μ_i and σ_i are the mean location and covariance matrix of the i th bivariate Gaussian respectively. If the bounding area were infinite, that is $x_{\min} = y_{\min} = -\infty$ m and $x_{\max} = y_{\max} = \infty$ m, then $\sum p(\mathbf{x}) = 1$. However, as can be seen from Figure 1, the area enclosed by the rectangular bounds contain less than this. Section 3.1.3 further discusses how this is handled such that the available probability is normalized.

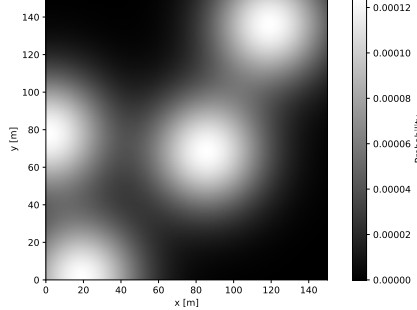


Figure 1: An example multi modal bivariate Gaussian PDM

3.1.3 Reward

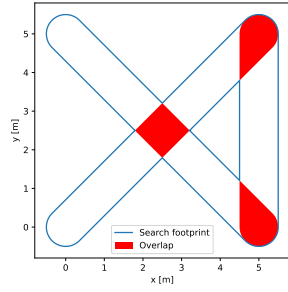
As the agent moves a constant distance sm every step, it is assumed that the camera follows this path continuously at a fixed height whilst pointing straight down at all times. Therefore, to represent the *seen area* for a given path at time-step t , the path is buffered by $R_{\text{buffer}}m$ to give the polygon h_t . All probability from the PDM enclosed within h_t is then *seen* and denoted by p_t . This value, the seen probability, is calculated through

$$I(H) = \int_H p(\mathbf{x}) dH \quad (5)$$

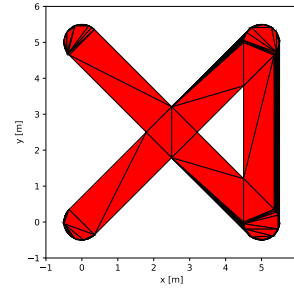
with $H = h_t$. $p(\mathbf{x})$ is from Equation 3. Thusly,

$$p_t = I(h_t) \quad (6)$$

The integral is calculated using a cubature integration scheme^[8,4] with constrained Delaunay triangulation^[3] to subdivide H into triangles as seen in Figure 2b.



(a) An example of how the buffered path polygon h automatically deals with re-seen areas. Note that the highlighted areas are just for demonstration and are not a part of the algorithm.



(b) The polygon from Figure 2a triangulated using the Delaunay constrained triangulation.

Figure 2: Visualizations of concepts related to the buffered polygon representation of the seen area.

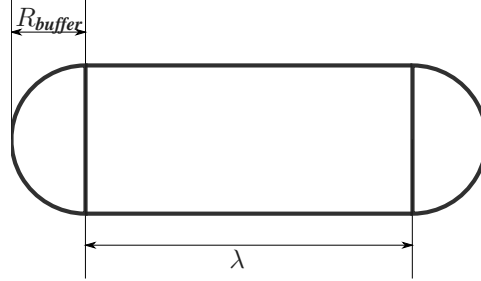


Figure 3: The anatomy of the area calculation of an isolated step of length λ with buffer R_{buffer} as used in Equation 9.

Other than allowing easy calculation of the accumulated probability, the buffering of the path prevents revisiting of an area contributing the same probability multiple times. This can be seen at the cross-over point (2.5, 2.5)m in Figure 2a.

In order to correlate action to reward, only the additional probability that has been accumulated

$$\Delta p_t = p_t - p_{t-1} \quad (7)$$

is used. To normalize this value, the scaling constant k is introduced. This scales Δp_t by the ratio of the area of an isolated step d_m to the area of the total search area a_m^2 . This is defined as

$$k = \frac{a_{area}}{2(\frac{1}{2}\pi R_{buffer}^2) + 2R_{buffer}\lambda} \quad (8)$$

$$= \frac{a_{area}}{R_{buffer}(\pi R_{buffer} + 2\lambda)} \quad (9)$$

with further spatial definitions from Figure 3.

As highlighted in Section 3.1.2, the enclosed probability by the bounds is not equal to 1. To handle this, Δp_t is scaled by the total available probability within the search area $p_A = I(A)$. Combining p_A with Equation 7 and Equation 9, gives the reward

$$r = \frac{k}{p_A} \Delta p_t \quad (10)$$

The enclosed probability can then be used to calculate the probability efficiency at time-step t with

$$e_{p,t} = \frac{p_t}{p_A} \quad (11)$$

and $e_{p,t} \leq 1$.

Finally, reward shaping is used to discourage future out-of-bounds actions and to penalize visiting areas of low probability or revisiting previously seen sections. The latter is easily handled by the buffering of the path as seen in Figure 2a, where the areas highlighted in red will contribute nothing to the reward resulting in a penalty of $-w_{oob}$. The augmented reward r' is then defined as

$$r' = \begin{cases} -w_{oob}, & \mathbf{x}_t \notin [x_{\min}, x_{\max}] \times [y_{\min}, y_{\max}] \\ w_r r, & \Delta p_t > \epsilon \\ -w_0, & \text{else} \end{cases} \quad (12)$$

3.2 Training Algorithm

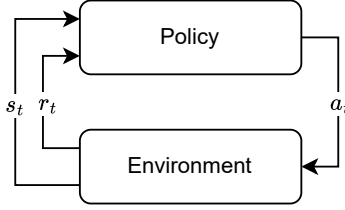


Figure 4: Top-level representation of a typical reinforcement learning data flow. The agent is also commonly referred to as the policy

SAC^[12] is a DRL algorithm well-suited for continuous control problems like drone navigation^[16]. It tackles the challenge of exploration vs exploitation by simultaneously maximizing expected reward and entropy. Entropy encourages exploration of the environment, preventing the policy from getting stuck in local optima. SAC achieves this by learning a policy, multiple Q-functions to evaluate actions, and a temperature parameter^[13] that controls the trade-off between exploration and exploitation. Figure 4 outlines the iterative process of reinforcement learning, where the policy is used to generate actions a_t and the environment then provides the resultant observation s_t and reward r_t .

3.2.1 Policy Architecture

The core of the policy is comprised of a fully connected network with N_{layers} layers, each with a width of N_{width} . This is given an input from the Feature Extractor (FE) which is further subdivided into five sub-FEs; path history s_{path} , PDM parameters s_{PDM} , out-of-bounds s_{oob} , and number of steps s_{steps} . The corresponding state observations for each of the sub-FEs is defined in Table 1 and each observation is linearly normalized. This results in a total of $2N_{\text{waypoints}} + 6G + 4$ observation inputs.

Table 1: Definition of the five state observations

Sub-state	Symbol	Definition	Shape
Path	s_{path}	$([\mathbf{x}_0, \dots, \mathbf{x}_t] \parallel \mathbf{0}^{2 \times N_{\text{waypoints}} - t})^T$	$(2, N_{\text{waypoint}})$
PDM	s_{PDM}	$[\mu_0, \sigma_0, \dots, \mu_G, \sigma_G]^T$	$(2, 3G)$
Position	s_{pos}	\mathbf{x}_t	$(1, 2)$
Out-of-bounds	s_{oob}	$\mathbf{x}_t \in [x_{\min}, x_{\max}] \times [y_{\min}, y_{\max}]$	$(1, 1)$
Number of steps	s_{steps}	t	$(1, 1)$

The policy architecture designed to handle this observation is defined in Figure 5. The sub-FE for the r_{path} state observation is of particular note as it uses a 2D CNN architecture based on work by Mnih et al.^[22].

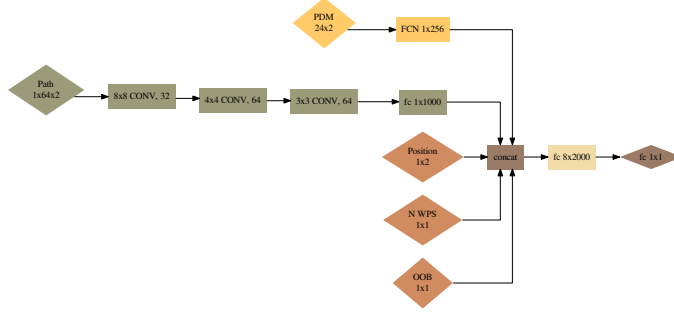


Figure 5: Policy network architecture

Table 2: Number of runs per algorithm

Method	N
LHC_GW_CONV	5×10^3
Lawnmower	5×10^3
SAC-FS-CNN	10×10^3

4 Results

4.1 Experimental setup

In order to effectively benchmark the proposed algorithms, two additional baselines are implemented; lawnmower^[10] and LHC_GW_CONV^[20]. These were chosen due to the former being ubiquitous for coverage planning, and the latter being a optimisation-based implementation that struggles to fully explore the PDM. To ensure compatibility in the comparison to the proposed algorithm, the parallel lines for lawnmower are offset by the step size λ and the grid dimensions for LHC_GW_CONV are $(x_{\max} - x_{\min}, y_{\max} - y_{\min})/\lambda$. The maximum number of waypoints N_{waypoint} are converted to a maximum distance $D_{\max} = \lambda N_{\text{waypoint}}$ and the generated paths are truncated at this point.

The results for the algorithm implemented in this research, titled *SAC-FS-CNN* from here on in, is the cumulation of three separate training runs with random starting seeds. This aligns with the best practices outlined by Agarwal et al.^[11] to ensure robust analysis for DRL results. Each model was trained for a minimum of 21 days (5×10^8 global steps) with 32 workers on a local Ubuntu 22.04 machine with a AMD Ryzen 9 5950X CPU with a NVIDIA RTX A6000 GPU and 64GB of RAM.

One evaluation of an algorithm involves generating the random PDM, then creating the resultant search path. This is labelled one run. Table 2 shows the number of runs undertaken per algorithm and this generated data is base of the following analysis.

4.2 Probability Over Distance (POD)

Maximising the probability efficiency (Equation 11) at all times is critical. This directly correlates to increasing the chances of finding a missing person in a shorter time. It is important for the POD of SAC-FS-CNN to out-perform the benchmark algorithms at all times. If this is not the case, the search algorithm selection becomes dependent on the endurance and mission. However, if the POD is better at all times then one algorithm will be superior no matter the application. To calculate the POD, the probability efficiency is evaluated at

$$d = \frac{(N_{\text{steps}} - i)D}{N_{\text{steps}}} \forall i \in \{N_{\text{steps}}, N_{\text{steps}} - 1, \dots, 1, 0\} \quad (13)$$

with $N_{\text{steps}} = 50$.

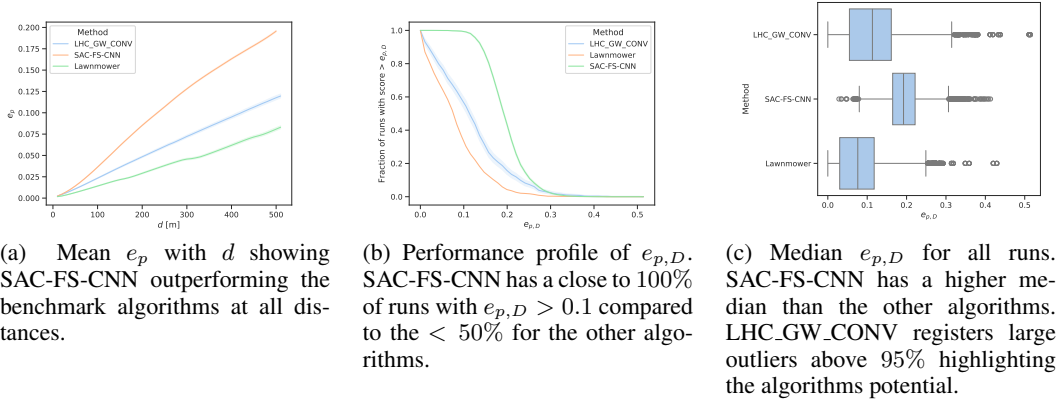


Figure 6: Probability efficiency analysis over all runs. The shaded regions in Figure 6a and Figure 6b show the 95% confidence interval.

Table 3: Mean POD performance metrics with the standard deviation as error.

Method	p_D	$e_{p,D}$	N
LHC_GW_CONV	0.09 ± 0.06	0.12 ± 0.08	9.3×10^3
Lawnmower	0.06 ± 0.04	0.08 ± 0.06	10×10^3
SAC-FS-CNN	0.15 ± 0.04	0.19 ± 0.04	9.8×10^3

From Figure 6a it is clear that SAC-FS-CNN sufficiently outperforms the benchmark algorithms at all distances. This is further highlighted by the $e_{p,D}$ for SAC-FS-CNN at 238% of that of lawnmower, and 158% for LHC_GW_CONV from Table 3. This is corroborated by the median $e_{p,D}$ values in Figure 6c. Notably, however, LHC_GW_CONV has a substantial amount of high $e_{p,D}$ outliers.

Likewise, the performance profile from Figure 6b follows the trend. It can be seen that SAC-FS-CNN has close to 100% of runs with $e_{p,D} > 0.1$ and 50% at approximately $e_{p,D} > 0.2$. This aligns with results from Figure 6c and Table 3.

4.3 Distance To Find (DTF) and Percentage Found (PF)

Whilst POD shows the theoretical effectiveness of an algorithm, the intended use-case is finding a missing person whilst searching within a bounded area. The mission statement is reducing the time it takes to find the potentially vulnerable person to save lives.

To quantify this requirement, we introduce DTF and PF. The former gives a clear answer on the capabilities on the various algorithms, whilst the latter should align with the POD results from Table 3 for validation.

Firstly, Gumbel-Softmax^[19] is used to sample N_{samples} positions from the PDM to give the set $\chi \in \mathbb{R}^{2 \times N_{\text{samples}}}$ containing all samples. The path is then traversed in incremental steps using Equation 13 with $N_{\text{step}} = 1 \times 10^4$. At each step, a euclidean distance check is done from the current position \mathbf{x} to each entry in χ with any points within R_{buffer} being marked as seen. The updated set of positions to search for in the next step is then

$$\chi' = \{\chi_i \in \chi : \|\mathbf{x} - \chi_i\| > R_{\text{buffer}}\} \quad (14)$$

From Figure 7, it is clear to see that SAC-FS-CNN outperforms the benchmark algorithms with a lower median DTF as well as a lower inter-quartile range. Table 4 shows that the mean DTF is 15.22% lower than lawnmower, and 4.07% lower than LHC_GW_CONV. This is in line with expectations from the results in Section 4.2. Likewise, the PF values closely match to the $e_{p,D}$ values from Table 3 showing that this test correlates to the theory.

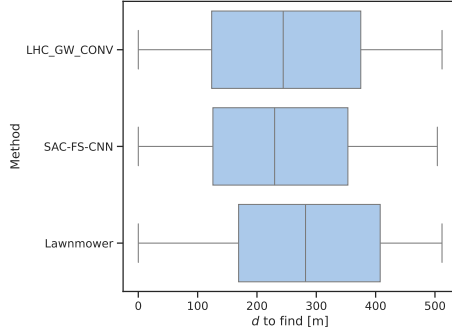


Figure 7: Median d to find. Similar 5% and 95% confidence markers across the algorithms shows the broad distribution of results from this experiment. SAC-FS-CNN ultimately has the lowest median score.

Table 4: DTF performance metrics

Method	PF [%]	Mean DTF [m]	N
LHC_GW_CONV	11.86 ± 0.32	249.37 ± 145.70	5×10^6
Lawnmower	7.77 ± 0.27	282.63 ± 146.62	5×10^6
SAC-FS-CNN	19.00 ± 0.39	239.61 ± 138.16	10×10^6

5 Limitations

DRL search mission planning holds promise, but limitations exist. The proposed environment assumes a flat, confined world, hindering performance in complex environments with varying altitudes. Similarly, a limited camera view restricts the agent’s ability to look around, as does the fixed height constraint. Additionally, fixed waypoint spacing and difficulty scaling to different mission sizes reduce flexibility and adaptability. Likewise, scaling to higher $N_{gaussian}$ values, or other PDM representations also presents the same issues. Further research is needed to address these limitations and unlock DRL’s fully for robust search mission planning in the real world.

6 Conclusion

Our research investigated the potential application of DRL for mission planning in WiSAR operations, leveraging a priori information. This was identified as a solution to the challenge of maximizing accumulated probability over a given area due to the powerful capabilities of machine learning to identify patterns and make generalizations in complex tasks.

The results indicate that DRL can outperform benchmark algorithms in the probability efficiency by up to 250% for lawnmower, and 166% for LHC_GW_CONV . A similar trend is identified when comparing mean distance-to-find with DRL outperforming the aforementioned algorithms by 15.22% and 4.07% respectively. The critical result, however, was that DRL found 160% more simulated missing people than LHC_GW_CONV . This translates to a substantial advantage in locating missing individuals, potentially saving countless lives during WiSAR operations.

However, alongside these promising advancements, ethical considerations regarding DRL-powered drones in WiSAR require careful consideration. Unauthorized surveillance could lead to privacy violations, while noise pollution might disrupt wilderness areas. Furthermore, over-reliance on this technology might lead to overlooking vital details or malfunctions during critical rescue missions. By recognizing these potential drawbacks, we can ensure a more balanced and responsible approach to this promising technology.

Our research focused on simulations, highlighting the need for further studies to evaluate DRL in real-world scenarios with more complex environmental factors. Likewise, a more representative drone model should be tested to ensure compatibility between generated and physically feasible

paths. This step is vital to ensure a level of confidence that the generated paths do in fact have the capabilities to increase search performance. Without this, the generated paths could potentially hinder rather than assist fast and efficient WiSAR in the real world.

The integration of DRL into WiSAR mission planning holds great potential for the future of search, offering a powerful tool with potential to significantly increase the success rate of WiSAR efforts.

References

- [1] Rishabh Agarwal, Max Schwarzer, Pablo Samuel Castro, Aaron Courville, and Marc G. Belle-mare. Deep Reinforcement Learning at the Edge of the Statistical Precipice, January 2022.
- [2] Severin Carrell. Flying to the rescue: Scottish mountain teams are turning to drones. *The Guardian*, January 2022. ISSN 0261-3077.
- [3] L. Paul Chew. Constrained delaunay triangulations. *Algorithmica*, 4(1-4):97–108, March 2023. ISSN 0178-4617. doi: 10.1007/BF01553881.
- [4] Ronald Cools, Luc Pluym, and Dirk Laurie. Algorithm 764: Cubpack++: A C++ package for automatic two-dimensional cubature. *ACM Transactions on Mathematical Software*, 23(1): 1–15, March 1997. ISSN 0098-3500. doi: 10.1145/244768.244770.
- [5] Dariush Ebrahimi, Sanaa Sharafeddine, Pin-Han Ho, and Chadi Assi. Autonomous UAV Trajectory for Localizing Ground Objects: A Reinforcement Learning Approach. *IEEE Transactions on Mobile Computing*, 20(4):1312–1324, April 2021. ISSN 1558-0660. doi: 10.1109/TMC.2020.2966989.
- [6] Jan-Hendrik Ewers, David Anderson, and Douglas Thomson. GIS Data Driven Probability Map Generation for Search and Rescue Using Agents. In *IFAC World Congress 2023*, pages 1466–1471, 2023. doi: 10.1016/j.ifacol.2023.10.1834.
- [7] Jan-Hendrik Ewers, David Anderson, and Douglas Thomson. Optimal path planning using psychological profiling in drone-assisted missing person search. *Advanced Control for Applications*, page e167, September 2023. ISSN 2578-0727, 2578-0727. doi: 10.1002/adc2.167.
- [8] Jan-Hendrik Ewers, Swinton Sarah, David Anderson, McGookin Euan, and Douglas Thomson. Enhancing Reinforcement Learning in Sensor Fusion: A Comparative Analysis of Cubature and Sampling-based Integration Methods for Rover Search Planning, May 2024.
- [9] Roy Fox, Ari Pakman, and Naftali Tishby. Taming the Noise in Reinforcement Learning via Soft Updates, March 2017.
- [10] Enric Galceran and Marc Carreras. A survey on coverage path planning for robotics. *Robotics and Autonomous Systems*, 61(12):1258–1276, December 2013. ISSN 09218890. doi: 10.1016/j.robot.2013.09.004.
- [11] Yaqing Guo and Wenjian Wang. A robust adaptive linear regression method for severe noise. *Knowledge and Information Systems*, 65(11):4613–4653, November 2023. ISSN 0219-3116. doi: 10.1007/s10115-023-01924-4.
- [12] Tuomas Haarnoja, Aurick Zhou, Pieter Abbeel, and Sergey Levine. Soft Actor-Critic: Off-Policy Maximum Entropy Deep Reinforcement Learning with a Stochastic Actor, August 2018.
- [13] Tuomas Haarnoja, Aurick Zhou, Kristian Hartikainen, George Tucker, Sehoon Ha, Jie Tan, Vikash Kumar, Henry Zhu, Abhishek Gupta, Pieter Abbeel, and Sergey Levine. Soft Actor-Critic Algorithms and Applications, January 2019.
- [14] Amanda Hashimoto, Larkin Heintzman, Robert Koester, and Nicole Abaid. An agent-based model reveals lost person behavior based on data from wilderness search and rescue. *Scientific Reports*, 12(1):5873, December 2022. ISSN 2045-2322. doi: 10.1038/s41598-022-09502-4.

- [15] C. Donald Heth and Edward H. Cornell. Characteristics of Travel by Persons Lost in Albertan Wilderness Areas. *Journal of Environmental Psychology*, 18(3):223–235, September 1998. ISSN 0272-4944. doi: 10.1006/jevp.1998.0093.
- [16] Elia Kaufmann, Leonard Bauersfeld, Antonio Loquercio, Matthias Müller, Vladlen Koltun, and Davide Scaramuzza. Champion-level drone racing using deep reinforcement learning. *Nature*, 620(7976):982–987, August 2023. ISSN 1476-4687. doi: 10.1038/s41586-023-06419-4.
- [17] Diederik P. Kingma and Jimmy Ba. Adam: A Method for Stochastic Optimization, January 2017.
- [18] R. Koester, Donald C. Cooper, J. R. Frost, and R. Q. Robe. Sweep Width Estimation for Ground Search and Rescue. *undefined*, 2004.
- [19] Jiefeng Li, Tong Chen, Ruiqi Shi, Yujing Lou, Yong-Lu Li, and Cewu Lu. Localization with Sampling-Argmax, October 2021.
- [20] Lanny Lin and Michael A. Goodrich. UAV intelligent path planning for wilderness search and rescue. *2009 IEEE/RSJ International Conference on Intelligent Robots and Systems, IROS 2009*, 0(1):709–714, 2009. doi: 10.1109/IROS.2009.5354455.
- [21] Lanny Lin and Michael A. Goodrich. Hierarchical Heuristic Search Using a Gaussian Mixture Model for UAV Coverage Planning. *IEEE Transactions on Cybernetics*, 44(12):2532–2544, December 2014. ISSN 2168-2267, 2168-2275. doi: 10.1109/TCYB.2014.2309898.
- [22] Volodymyr Mnih, Koray Kavukcuoglu, David Silver, Andrei A. Rusu, Joel Veness, Marc G. Bellemare, Alex Graves, Martin Riedmiller, Andreas K. Fidjeland, Georg Ostrovski, Stig Petersen, Charles Beattie, Amir Sadik, Ioannis Antonoglou, Helen King, Dharshan Kumaran, Daan Wierstra, Shane Legg, and Demis Hassabis. Human-level control through deep reinforcement learning. *Nature*, 518(7540):529–533, February 2015. ISSN 1476-4687. doi: 10.1038/nature14236.
- [23] James W. Mock and Suresh S. Muknahallipatna. A Comparison of PPO, TD3 and SAC Reinforcement Algorithms for Quadruped Walking Gait Generation. *Journal of Intelligent Learning Systems and Applications*, 15(1):36–56, February 2023. doi: 10.4236/jilsa.2023.151003.
- [24] Michael Morin, Irène Abi-Zeid, and Claude-Guy Quimper. Ant colony optimization for path planning in search and rescue operations. *European Journal of Operational Research*, 305(1): 53–63, February 2023. ISSN 0377-2217. doi: 10.1016/j.ejor.2022.06.019.
- [25] OpenAI. Dota 2 with Large Scale Deep Reinforcement Learning. *arXiv:1912.06680 [cs]*, December 2019. doi: 10.48550/arXiv.1912.06680.
- [26] Ashley Peake, Joe McCalmon, Yixin Zhang, Benjamin Raiford, and Sarra Alqahtani. Wilderness Search and Rescue Missions using Deep Reinforcement Learning. In *2020 IEEE International Symposium on Safety, Security, and Rescue Robotics (SSRR)*, pages 102–107, November 2020. doi: 10.1109/SSRR50563.2020.9292613.
- [27] Antonin Raffin, Ashley Hill, Adam Gleave, Anssi Kanervisto, Maximilian Ernestus, and Noah Dormann. Stable-Baselines3: Reliable Reinforcement Learning Implementations. *Journal of Machine Learning Research*, (22), 2021.
- [28] John Schulman, Filip Wolski, Prafulla Dhariwal, Alec Radford, and Oleg Klimov. Proximal Policy Optimization Algorithms, August 2017.
- [29] Ljiljana Šerić, Tomas Pinjušić, Karlo Topić, and Tomislav Blažević. Lost Person Search Area Prediction Based on Regression and Transfer Learning Models. *ISPRS International Journal of Geo-Information*, 10(2):80, February 2021. ISSN 2220-9964. doi: 10.3390/ijgi10020080.
- [30] Louise Skeleton and Craig Smith. Remotely Piloted Aircraft System (RPAS) Evaluation Report. Technical report, Scottish Police Authority, SPA Policing Performance Committee, November 2020.

- [31] Gregory Snyder, Sachin Shrivastava, Dylan Morrison-Fogel, and Zhuoyuan Song. Path Planning for Optimal Coverage of Areas with Nonuniform Importance, December 2021.
- [32] Abhishek Subramanian, Ryan Alimo, Thomas Bewley, and Philip Gill. A Probabilistic Path Planning Framework for Optimizing Feasible Trajectories of Autonomous Search Vehicles Leveraging the Projected-Search Reduced Hessian Method. In *AIAA Scitech 2020 Forum*, Orlando, FL, January 2020. AIAA, American Institute of Aeronautics and Astronautics. ISBN 978-1-62410-595-1. doi: 10.2514/6.2020-0987.
- [33] Muhammad Talha, Aya Hussein, and Mohammed Hossny. Autonomous UAV Navigation in Wilderness Search-and-Rescue Operations Using Deep Reinforcement Learning. In Haris Aziz, Débora Corrêa, and Tim French, editors, *AI 2022: Advances in Artificial Intelligence*, Lecture Notes in Computer Science, pages 733–746, Cham, 2022. Springer International Publishing. ISBN 978-3-031-22695-3. doi: 10.1007/978-3-031-22695-3_51.
- [34] Sonia Waharte and Niki Trigoni. Supporting Search and Rescue Operations with UAVs. In *2010 International Conference on Emerging Security Technologies*, pages 142–147. University of Oxford, September 2010. doi: 10.1109/EST.2010.31.
- [35] Jie Xu, Tao Du, Michael Foshey, Beichen Li, Bo Zhu, Adriana Schulz, and Wojciech Matusik. Learning to fly: Computational controller design for hybrid UAVs with reinforcement learning. *ACM Transactions on Graphics*, 38(4):1–12, August 2019. ISSN 0730-0301, 1557-7368. doi: 10.1145/3306346.3322940.
- [36] Peng Yao, Zexiao Xie, and Ping Ren. Optimal UAV Route Planning for Coverage Search of Stationary Target in River. *IEEE Transactions on Control Systems Technology*, 27(2):822–829, March 2019. ISSN 1063-6536, 1558-0865, 2374-0159. doi: 10.1109/TCST.2017.2781655.
- [37] Burak Yuksek, Mustafa Umut Demirezen, Gokhan Inalhan, and Antonios Tsourdos. Cooperative Planning for an Unmanned Combat Aerial Vehicle Fleet Using Reinforcement Learning. *Journal of Aerospace Information Systems*, 18(10):739–750, 2021. ISSN 1940-3151. doi: 10.2514/1.1010961.

A Parameters

Table 5: Simulation parameters used for this study

Parameter	Value	Units
N_{gaussian}	4	
σ_i	$\text{diag}(500, 500)$	
x_{\min}, y_{\min}	0	m
x_{\max}, y_{\max}	150	m
λ	8	m
R_{buffer}	2.5	m
N_{waypoint}	64	
ϵ	0.1	
w_{oob}	1.0	
w_r	0.5	
w_0	0.5	

B Policy Network Design

Search planning is a abstract task compared to point-to-point or coverage planning. Therefore, a parameter sweep for the network architecture was performed to ensure sufficient capabilities. A core aspect of this was the large path history observation with $2N_{\text{waypoint}}$ elements since the policy must be able to learn how to avoid crossing over itself to avoid penalties.

Table 6: SAC hyperparameters used for this study from empirical testing. Other variables were kept at the default values from Raffin et al.^[27] v2.1.0

Hyperparameter	Value
Learning rate	1×10^{-6}
Optimizer	Adam ^[17]
Batch size	1024
Learning starts	8192
Buffer size	5×10^6
Training frequency	10
Gradient steps	50
τ	1×10^{-4}

In this sweep four variables were tuned; number of layers N_{layers} , layer width N_{width} , path output feature dimension, and path feature extractor. N_{layers} and N_{width} correlate to the core policy network, and the other feature extractors are left unchanged and can be seen in Figure 5. The ranges of these sweeps can be seen from Figure 9. The SAC hyperparameters from Table 6 were used for all runs.

There were three path feature extractors that were tested. A standard FCN-based approach (Figure 8a), a 2D CNN from Mnih et al.^[22] (Figure 8c), and a 1D CNN variant (Figure 8b).

In total, 39 runs were completed over 12 days in the same computational environment as outlined in Section 4.1. A random sampling strategy was used to ensure broad coverage of the hyperparameter space. Results from this, with a fitted ordinary least squares (OLS) linear regression where applicable, can be seen in Figure 9.

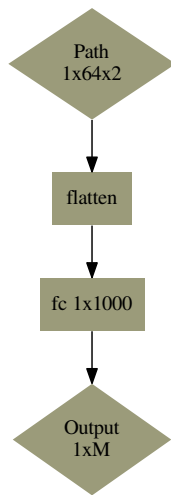
From the results in Figure 9a and Figure 9b it is evident that a deeper, wider network leads to better results. However, Figure 9b does taper off in performance after $N_{\text{layers}} = 8$ with similar results. The overall number of parameters per result were calculated and plotted in Figure 10. This confirms the result that a larger policy network is better. A network size of 8×2000 was selected as seen in Figure 5.

Results from the path output feature dimension in Figure 9d would be expected to show similar results. However, the OLS has a downward trend implying lower values for being better. Yet the fitted model did not exhibit statistically significant explanatory power, with a p-value of 0.393. For comparison, the p-values for N_{layers} and N_{width} were 0.00522 and 0.00339 respectively and are well below the standard test p-value of 0.05. Thus, a path output feature dimension of 1000 was selected.

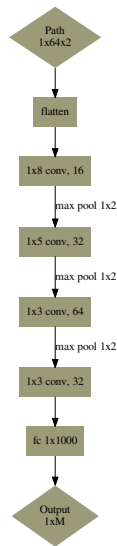
Finally, the result for the path feature extraction method in Figure 9c highlight that the 2D CNN feature extractor yields the highest median $e_{p,D}$. However, the 1D CNN median result is very similar. A p-value was calculated against each distribution to determine if the results were significantly different.

Figure 11 shows that distribution of 2D CNN results is statistically significantly different from the rest with p-values below 0.05. Therefore, 2D CNN was used as the path feature extractor as seen in Figure 5.

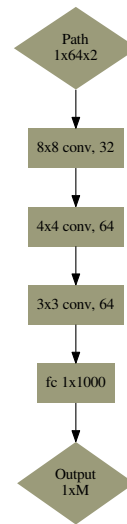
A limitation of this analysis approach is the need to assume that the results are independent. This is of course not necessarily true as changing the feature extractor might change the requirements for N_{width} . Furthermore, the high p-value score for the path feature extraction method implies that more runs could have been undertaken. It may also imply that this value is not important to the network. However, a more complex analysis is outwith the scope of this study.



(a) Single-layer FCN path feature extractor

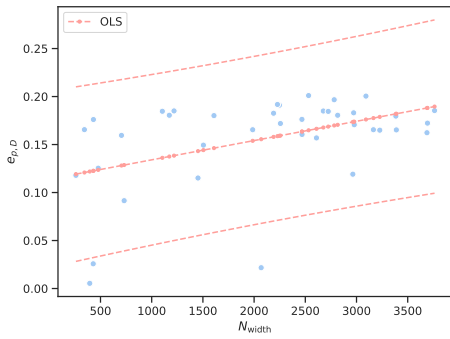


(b) 1D convolution path feature extractor

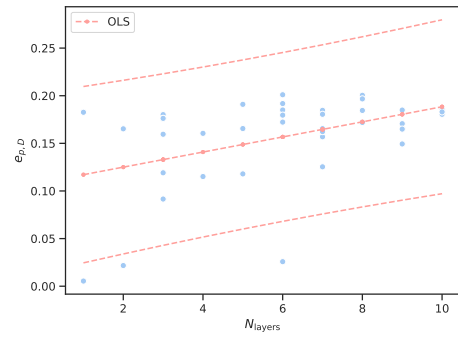


(c) 2D convolution path feature extractor

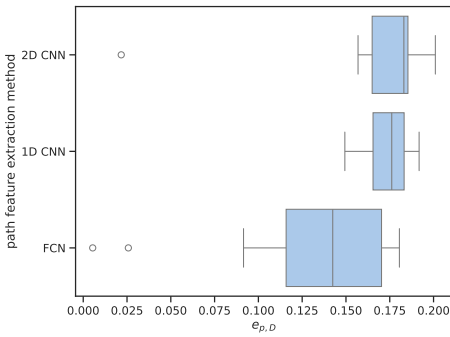
Figure 8: Architectures of the three candidate path feature extractors. M is the path output feature dimension.



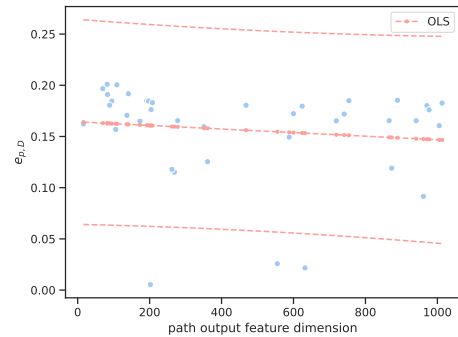
(a) N_{width}



(b) N_{layer}



(c) Path feature extraction method



(d) Path feature extraction method output dimension

Figure 9: Ordinary least squares (OLS) linear regression fitted to the $e_{p,D}$ results from the hyperparameter sweep.

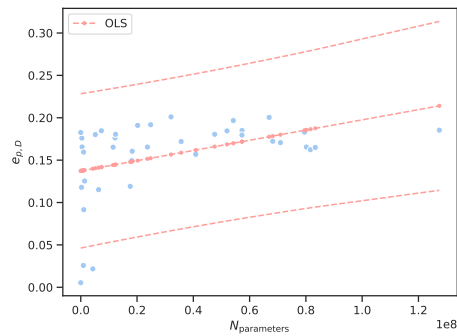


Figure 10: $e_{p,D}$ with the number of parameters within the policy network. This value was derived from Figure 9a and Figure 9b.

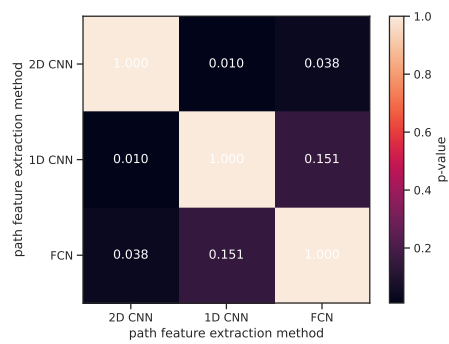


Figure 11: p-value matrix from comparing the result distributions categorized by feature extraction method.